ELSEVIER

Coordination Chemistry Reviews
198 (2000) 265–295

COORDINATION CHEMISTRY REVIEWS

www.elsevier.com/locate/ccr

Theoretical studies on effective spin interactions, spin alignments and macroscopic spin tunneling in polynuclear manganese and related complexes and their mesoscopic clusters

H. Nagao, M. Nishino, Y. Shigeta, T. Soda, Y. Kitagawa, T. Onishi, Y. Yoshioka, K. Yamaguchi *

Department of Chemistry, Graduate School of Science, Osaka University, Toyonaka, Osaka 560-0043, Japan

Received 8 June 1999; accepted 14 December 1999

Contents

* Corresponding author. Fax: +81-6-68505550.
E-mail address: yama@chem.sci.osaka-u.ac.jp (K. Yamaguchi)

PII: S0010-8545(00)00231-9

Abstract

Theoretical efforts to investigate molecular magnetic materials are reviewed mainly from the viewpoint of our interest. Ab initio calculations of effective exchange interactions between spins are performed for H–H, H–He–H and simplified models of binuclear manganese and related complexes by using the spin unrestricted Hartree–Fock (UHF) and spin-polarized density functional (DFT), and UHF plus DFT hybrid methods. The scope and limitation of these broken-symmetry approaches are briefly discussed in relation to several computational schemes of effective exchange integrals (J_{ab}). The calculated J_{ab} values for the three systems are summarized for comparison of the computational methods. The natural orbitals (UNO or DNO) of the UHF and DFT solutions for magnetic clusters are determined by diagonalizing their first-order density matrices. They are used for MO-theoretical interpretation of superexchange interactions. The effective spin Hamiltonians such as the Heisenberg model are constructed for polynuclear complexes assuming the calculated and experimental effective exchange integrals. The macroscopic quantum tunneling (MQT) and coherence (MQC) of spins in the manganese oxide clusters are analyzed using the Heisenberg model, and the tunneling rate of spins is calculated by the coherent state path integral method. The topological rules for MQT and MQC are derived from this analysis. The path integral formulations are extended to tunneling probabilities for clusters of clusters and spin lattices with mesoscopic size. The resulting ideas are also applied to the molecular design of mesoscopic clusters of clusters in intermediate and strong correlation regimes. The active control of spins are finally discussed from the viewpoint of functionalities in molecular and biological materials, and technological applications of mesoscopic molecular magnets to quantum computing.

Keywords: Spin interactions; Spin alignments; Macroscopic spin tunneling

1. Introduction

During the past decade, the bottom-up strategy for the creation of new materials from molecular blocks has accepted broad interest since the well-developed bottom-down approach by the use of conventional semiconductor and metals often suffers from technological difficulties in mesoscopic (nanoscale) regimes, in which quantum effects play crucial roles for electron transport and magnetism. From this viewpoint, polynuclear transition metal complexes have potential applications as building blocks for new electronic, magnetic and optical materials. In fact, many transition metal spin clusters have been synthesized [1–3], and general spin align-

ment, spin frustration and spin tunneling in these species have been investigated both experimentally and theoretically. For example, magnetic measurements of the vanadium oxide cluster ($V_{15}O_{42}$) have shown a noncolinear spin alignment in the ground state [4]. Similarly Vincent and Christou [5] have reported that manganese oxide clusters with triangular, butterfly, and cubic molecular structures have indicated peculiar and complex magnetic behaviors.

The magnetic properties of transition metal complexes have been investigated by the use of the Heisenberg–Dirac–van Vleck spin Hamiltonian [6]. For example, the effective exchange interaction between localized spins in binuclear transition metal complexes is described by the total spin form of the spin-coupling Hamiltonian [7]

$$\boldsymbol{H}(HB) = J_{ab}\boldsymbol{S}_a \cdot \boldsymbol{S}_b \tag{1}$$

where J_{ab} is the orbital-averaged effective exchange integral between the a-th and b-th metal sites with total spin operators $\boldsymbol{S}_a$ and $\boldsymbol{S}_b$. J_{ab} is often defined as $-2J'_{ab}$ [8–12]. Then the exchange split energy levels for binuclear transition metal complexes are given by

$$^{2S+1}E(\mathrm{HB}) = \frac{J_{ab}}{2}[S(S+1) - S_a(S_a+1) - S_b(S_b+1)] \tag{2}$$

where S_a and S_b are the magnitudes of spins $\boldsymbol{S}_a$ and $\boldsymbol{S}_b$ and S is the magnitude of the total-spin operators $\boldsymbol{S}$ of the systems,

$$S = |S_a - S_b|, \quad |S_a - S_b| + 1, \ldots, (S_a + S_b) \tag{3}$$

The effective exchange integral (J_{ab}) has been regarded as an empirical parameter, which is determined so as to reproduce the magnetic properties of transition metal complexes [8]. On the other hand, the sign of J_{ab} is qualitatively explained by considering spatial symmetries of magnetic d-orbitals [9,10] for transition metal complexes and magnetic p-orbitals for organic radical clusters [11,12]. Ab initio computations of J_{ab} are current topics as shown below.

Recently, several theoretical and experimental studies have been carried out for single molecule magnets. In 1980 Lis [13] first synthesized $Mn_{12}O_{12}$-$(CH_3COO)_{16}(H_2O)_4$ referred to as Mn_{12}, and has described a 12 ion manganese cluster, which contains eight Mn ions in the $+3$ oxidation state (spin $S = 2$) and four in the $+4$ state ($S = 3/2$). These ions are magnetically coupled to give a ground state with $S = 10$, giving rise to unusual magnetic relaxation properties. Since Mn_{12} was synthesized, magnetic properties such as magnetic quantum tunneling events of the Mn_{12}–Ac complex [14–18] have been investigated theoretically and experimentally. Sessoli et al. [15] have reported high-spin molecules such as $Mn_{12}O_{12}(O_2CR)_{16}(H_2O)_4$. The magnetization of the Mn_{12} cluster is highly anisotropic, and the magnetization relaxation time becomes very long at low temperature, showing the pronounced hysteresis. This behavior is not strictly analogous to that of a bulk ferromagnet, in which magnetization hysteresis results from the motion of domain walls. In Section 3, we will discuss the magnetization hysteresis in relation to the magnetic quantum tunneling and its rate [19–25].

In this review, we summarize our recent theoretical efforts to understand molecular magnetism in transition metal complexes. We first perform ab initio molecular orbital calculations of hydrogen molecule (H–H), H–He–H biradical and binuclear manganese complexes to examine effective exchange interactions between spins and to derive effective spin Hamiltonians. Next, we investigate the magnetic quantum tunneling of several Mn clusters with triangular, butterfly and tetrahedral structures etc. [26] and a cluster system of clusters in relation to the topological structures and integer or half-integer spins by using a coherent state path integral. General expressions of the imaginary time transition amplitude and the quantum magnetic tunneling rate [27] are calculated by means of the path integral representation of the nonlinear σ model [22,28–30], and effective Lagrangians for manganese clusters in the ground state are also derived to obtain a general expression of the imaginary time tunneling amplitude. Finally, we briefly discuss possibilities of quantum computing by the use of spin clusters.

2. Effective exchange interactions between spins

2.1. Computational schemes of effective exchange integrals

Recent development in computational quantum chemistry enables us to perform ab initio calculations of J_{ab} values in the Heisenberg model. These are classified into two types: one is the spin-symmetry adapted perturbational and configuration interaction (CI) approach [31–41], while the other is the broken-symmetry approach (BS) [42–67]. The former method is desirable for quantitative computations of J_{ab}, but it is hardly applicable to transition metal clusters because of high computational cost. As a result the latter BS (low cost) approach is used heavily for such systems, though the spin contamination problem occurs in the low-spin (LS) state [46,47,52]. Here, we examine the BS method, since it will be applicable even for large transition metal complexes of biological interest. Three typical computational schemes of J_{ab} have been presented by several groups as

$$J_{ab}^{(1)} = \frac{2[{}^{\mathrm{HS}}E(X) - {}^{\mathrm{LS}}E(X)]}{S_{\max}^2} \tag{4}$$

$$J_{ab}^{(2)} = \frac{2[{}^{\mathrm{HS}}E(X) - {}^{\mathrm{LS}}E(X)]}{S_{\max}(S_{\max}+1)} \tag{5}$$

$$J_{ab}^{(3)} = \frac{2[{}^{\mathrm{HS}}E(X) - {}^{\mathrm{LS}}E(X)]}{{}^{\mathrm{HS}}\langle s^2\rangle(X) - {}^{\mathrm{LS}}\langle s^2\rangle(X)} \tag{6}$$

where ${}^{Y}E(X)$ and ${}^{Y}\langle s^2\rangle(X)$ denote the total energy and total spin angular momentum for the spin state Y, respectively by the method X (UHF, DFT, etc.). Note that $J_{ab}^{(n)}$ ($n = 1$–3) is an average of all the exchange integrals (J_{ij}) between magnetic orbitals. The first scheme $J_{ab}^{(1)}$ has been derived by Ginsberg [49], Noodleman [50] and Davidson [53] (GND), while the second scheme $J_{ab}^{(2)}$ has been proposed by GND, Bencini [65] and Ruiz [66] (BR), and others. The last scheme $J_{ab}^{(3)}$ is given by

our approximate spin-projection (AP) procedure [52]. The second term in the denominator in Eq. (6) is responsible for the spin projection of the low spin (LS) solution, which often involves the higher-spin components as spin contamination. On the other hand, such a spin contaminant was negligible for the high-spin (HS) solution [46]. The $J_{ab}^{(3)}$ by AP is close to $J_{ab}^{(1)}$ by GND if ${}^{HS}\langle s^2\rangle \cong S_{max}(S_{max}+1)$ and ${}^{LS}\langle s^2\rangle \cong S_{max}$, where S_{max} is the size of spin for the high spin (HS) state. These relations are usually satisfied near the weak overlap (strong correlation) region. On the other hand, $J_{ab}^{(3)}$ becomes equivalent to $J_{ab}^{(2)}$ in the strong overlap (weak correlation) region, where ${}^{LS}\langle s^2\rangle \cong 0$.

In order to confirm the above relationships, we have calculated $J_{ab}^{(n)}$ ($n = 1$–3) for hydrogen molecule by using the UHF 6-311G** solutions for the singlet (LS) and triplet (HS) states. Fig. 1 shows the calculated results. From Fig. 1, the $J_{ab}^{(1)}$ and $J_{ab}^{(3)}$ values are quite similar in the dissociation region of H_2, while the $J_{ab}^{(2)}$ and $J_{ab}^{(3)}$ values are close in the strong overlap region. $J_{ab}^{(3)}$ reproduces the characteristic feature of J_{ab} by full CI in the whole region, although the $J_{ab}^{(1)}$ and $J_{ab}^{(2)}$ schemes break down in the strong and weak overlap regions, respectively. It is noteworthy that the $J_{ab}^{(3)}$ scheme is applicable to the spin-symmetry-adapted wavefunctions such as the full CI.

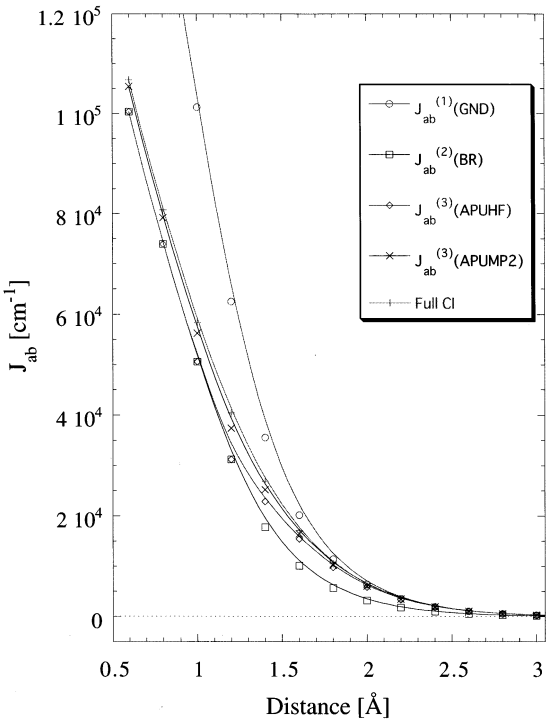

Fig. 1. Variations in the calculated $J_{ab}^{(n)}$ ($n = 1$–3) values with the interatomic distance of H2 by the UHF and UMP2/6-311G* methods (see text).

Eq. (6) can be applied to the UHF-based correlated wavefunctions; UHF Möller–Plesset (UMP), UHF coupled cluster (UCC), UHF quadratic CI (UQCI) etc. The correlation corrections by X = UMP, UCC or UQCI are usually crucial for quantitative calculations of J_{ab}. In fact $J_{ab}^{(3)}$ for H_2 by UMP2 is almost equivalent to the full CI value as shown in Fig. 1. However, post UHF methods are hardly applicable to large transition metal complexes. Therefore, DFT methods are heavily utilized for computations of such systems. However, conventional DFT (UBLYP, UB3LYP) are often biased to stabilize the low-spin (LS) state since the hybridization parameters involved in the exchange-correlation potentials are optimized to provide reliable bonding energies of closed-shell systems. Such DFT results for H_2 have been given in Ref. [60]. For theoretical investigation of molecular magnetism, the exchange-correlation parameters are therefore reoptimized to reproduce J_{ab} values of small binuclear transition metal systems by UCC, and the refined parameters are utilized for DFT calculations of J_{ab} values for larger systems [63]. In the DFT calculations, exchange-correlation potentials are generally defined by

$$E^{\mathrm{XC}} = C_1 E_X^{\mathrm{HF}} + C_2 E_X^{\mathrm{Slater}} + C_3 \Delta E_X^{\mathrm{Becke88}} + C_4 E_C^{\mathrm{VWN}} + C_5 \Delta E_C^{\mathrm{LYP}} \tag{7}$$

where the first and second terms in the right hand of Eq. (7) indicate HF and Slater exchange functionals, respectively. The third and fourth terms mean Becke's exchange corrections involving the gradient of the density and Vosko, Wilk, and Nusair (VWN) correlation functional, and the last term is the correlation correction of Lee, Yang, and Parr (LYP), which includes the gradient of the density. C_i ($i = 1, \ldots, 5$) are the mixing coefficients.

The H–He–H system has been utilized as a sample molecule to test the computational schemes for the superexchange interaction between hydrogen radicals via the helium atom. Table 1 summarizes the $J_{ab}^{(n)}$ ($n = 1$–3) values calculated by Eqs. (4)–(6). The 6-3111G* basis set is used for all the computations. From Table 1, the $J_{ab}^{(3)}$ value by each broken-symmetry method is smaller than the $J_{ab}^{(1)}$ one at $R_{\mathrm{H–He}} = 1.25$ Å, while $J_{ab}^{(3)} \cong J_{ab}^{(1)}$ at $R_{\mathrm{H–He}} = 2.0$ Å. This indicates that the overlap effect of magnetic orbitals is significant at the former conformation, while it is negligible at the latter one. The magnitude of $J_{ab}^{(n)}$ ($n = 1$–3) values at each conformation decrease in the order: UBLYP > UB3LYP > mUS2VWN > UB2LYP > UHF. The $J_{ab}^{(3)}$ values by UB2LYP and post UHF methods are close to those of 2×2 CI and full CI. On the other hand, UBLYP, UB3LYP and modified US2VWN (mUS2VWN) have overestimated the $J_{ab}^{(3)}$ values for H–He–H, while UHF has underestimated them. Therefore $J_{ab}^{(2)}$ by UBLYP, UB3LYP and US2VWN are rather similar to the corresponding CI values. This is the reason why the $J_{ab}^{(2)}$ scheme by the three DFT approximations is useful for H–He–H. However, it is noteworthy that their magnetic orbitals are remarkably delocalized, namely metallic, as compared with the CI and UMP*n* results [52,55,56].

2.2. Ab initio calculations of exchange-coupled systems

The computational scheme in Eq. (6) was first applied to direct exchange coupling between transition metal (M) and oxygen (O). Some of the transition metal oxygen bonds (M–O, M=O or M≡O) exhibited significant singlet biradical character ($\uparrow \cdot M\text{–}O \cdot \downarrow$), which is responsible for the radical reactivity such as hydrogen abstraction ability [52]. The ab initio UHF calculations were also carried out to elucidate the superexchange coupling between transition metal ions via the oxygen dianion; L_m M–X–M L_m (M = Cu, Mn, Cr, Ni; X = O^{2-}, O^-, F^-, Cl^- etc.; L_m = ligands) [52]. The J_{ab} value for Cu(II)–O–Cu(II) was abnormally large, showing the strongest superexchange coupling. By the use of this large J_{ab} value, we later estimated the transition temperature (T_c) for high-T_c superconductivity of copper oxides assuming that $T_c = cJ_{ab}$ (c is a constant) [55]. We have also examined several di-μ-bridged complexes $L_mM\text{–}X_2\text{–}ML_m$ such as the 2Fe–2S ferredoxin model [56,57]. The calculated J_{ab} values for the model systems were consistent with the available experiment results. The $J_{ab}^{(1)}$ values of 2Fe–2S and 4Fe–4S clusters by the DFT method [58,59] are about twice the experimental values, which is in agreement with the general trend in Table 1. In order to confirm this trend, we examine binuclear manganese complexes. Let us consider a model complex $[Mn_2^{IV}O_2(NHCHCO_2)_4]$ of $Mn_2O_2(pic)_4$ (pic = picolinic acid). The X-ray geometry of this parent compound was used for the DFT calculations of the model system [68]. The coordinate axis is taken as shown in Fig. 2(a). The ground state of Mn(IV) (d^3) is a quartet. Then, the manganese dimer $Mn(IV)_2$ is formally regarded as the d^3–d^3 exchange coupled system, and the magnetic orbitals should have the σ ($d_{z^2-x^2}$), π (d_{zy}) and δ (d_{xy}) symmetries as illustrated in Fig. 2(b), although they

Table 1
Effective exchange integrals (cm^{-1}) for H–He–H by several computational methods

Methods	$R_{HHe} = 1.25$			$R_{HHe} = 1.625$			$R_{HHe} = 2.000$		
	$J_{ab}^{(1)}$	$J_{ab}^{(2)}$	$J_{ab}^{(3)}$	$J_{ab}^{(1)}$	$J_{ab}^{(2)}$	$J_{ab}^{(3)}$	$J_{ab}^{(1)}$	$J_{ab}^{(2)}$	$J_{ab}^{(3)}$
BLYP	10782	5388	7616	1242	621	1198	139	69	138
UB3LYP	8733	4364	6941	1026	513	1001	114	57	114
mS2VWN[a]	8194	4095	6669	1006	503	982	114	57	114
B2LYP[b]	6895	3445	5989	818	409	806	88	44	88
UHF	3894	1946	3688	420	210	418	41	20	40
UMP2	4682	2341	4375	493	247	490	47	23	47
UMP4	5059	2530	4728	527	264	523	49	25	49
CASSCF[4,4][c]			4304			487			49
2 × 2 CI[d]			4782			530			52
Full CI[c]			4860			544			50

[a] B2LYP in our previous paper (Ref. [62]).
[b] Becke's half-and-half LYP (HHLYP in Ref. [66]).
[c] Ref. [66].
[d] Ref. [61].

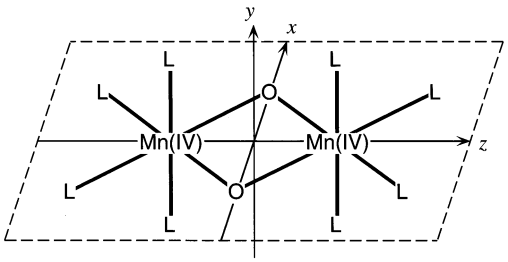

(a)

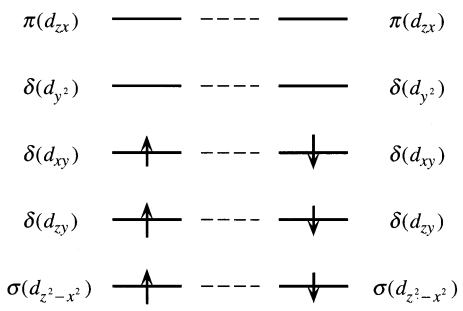

(b)

Fig. 2. Binuclear manganese complexes and magnetic orbitals. (a) Coordinate axis of model complex $[Mn_2^{IV}O_2(NHCHCO_2)_4]$ of $Mn_2O_2(pic)_4$ (pic = picolinic acid). (b) Magnetic orbitals of σ ($d_{z^2-x^2}$), π (d_{zy}) and δ (d_{xy}) symmetries.

are more or less delocalized over the ligands. In order to elucidate the bonding characteristics, the J_{ab} values were first calculated using Eqs. (4)–(6). Table 2 summarizes the effective exchange integrals of $[Mn_2^{IV}O_2(NCHCO_2)_4]$ by several hybrid DFT methods with different basis sets.

The $J_{ab}^{(n)}$ ($n = 1$–3) values for $[Mn_2^{IV}O_2(NHCHCO_2)_4]$ are not so different, because $S_{max} = 3$ for the binuclear Mn(IV) complex. The $J_{ab}^{(3)}$ value (568 cm^{-1}) by UBLYP with the MIDI basis set [62] was larger than the experimental value (174 cm^{-1}), in accordance with the general trend, while those of UB2LYP, USVWN and UB2VWN were too small (60 cm^{-1}). The former overestimated the electron delocalization, while the latter underestimated it. Therefore, the modified US2VWN (mUS2VWN) method, which was obtained by the intermediate mixing between these extremes as shown in Table 2, provided the reasonable J_{ab} values (188 cm^{-1}) as compared with the experiment. The large basis set with the *pdf*-polarization functions was necessary for quantitative purposes. Therefore, these refined methods would be used for quantitative DFT calculations of larger manganese complexes and crystals. Alternately, effective spin Hamiltonians with ab initio J_{ab} obtained for the nearest sites by ab initio calculation are useful for such systems at least for the purpose of qualitative explanation of the magnetism as shown below.

Table 2
Effective exchange integrals (cm^{-1}) for $[Mn_2^{IV}O_2(NHCHCO_2)_4]$ by several hybrid DFT methods

Parameter sets					$J_{ab}^{(1)}$	$J_{ab}^{(2)}$	$J_{ab}^{(3)}$	*cf*
c_1	c_2	c_3	c_4	c_5				
0.0	1.0	1.0	1.0	1.0	595	447	568	BLYP[a]
0.2	0.8	0.72	1.00	0.81	252	189	249	B3LYP[a]
					234	175	231	B3LYP[b]
0.5	0.5	0.5	1.0	1.0	62.3	46.7	61.5	B2LYP[a,c]
0.332	0.575	0.0	0.575	0.0	207	155	205	mS2VWN[a,d]
					189	142	188	mS2VWN[b,d]
0.5	0.5	0.5	1.0	0.0	57.5	43.2	56.8	B2VWN[a]
0.5	0.5	0.0	1.0	0.0	67.6	50.7	66.8	S2VWN[a]
							174	Exp.

[a] MIDI.
[b] MIDI + polarizations(pdf).
[c] Becke's half-and-half LYP(HHLYP in Ref. [66].
[d] B2LYP in our previous paper (Ref. [63]).

2.3. Magnetic orbitals

The modified DFT solutions of the binuclear complex were quite useful for deeper understanding of the superexchange interaction between Mn(IV) via an oxygen dianion, together with organic ligands. In order to obtain the MO theoretical explanation of the superexchange interaction, the natural orbitals (DNO) of the modified US2VWN (mUS2VWN) solutions were determined by diagonalizing their first-order density matrices as [62]

$$\rho(\boldsymbol{r}, \boldsymbol{r}') = \sum n_i \phi_i^*(\boldsymbol{r}) \phi_i(\boldsymbol{r}') \tag{8}$$

where n_i denotes the occupation number of DNO ϕ_i. The occupation numbers of bonding and antibonding DNOs were almost 2.0 and 0.0, respectively, except for the six magnetic DNOs, for which the occupation numbers were close to 1.0. The bonding DNOs with $n_i \approx 2.0$ are regarded as the closed-shell orbitals. On the other hand, the magnetic molecular orbitals for the up (α) and down (β) spins are obtained by almost equal mixing of the bonding and antibonding DNOs with $n_j \approx 1.0$

$$\psi_i^{\pm} = \cos\theta \phi_i \pm \sin\theta \phi_i^* \tag{9}$$

where $i = \sigma$, π or δ, and $\theta \approx 45°$.

The magnetic (localized) natural orbitals (MNO) are defined as the magnetic molecular orbitals at the strong correlation limit [62]

$$\phi_a = \frac{1}{\sqrt{2}}(\phi_i + \phi_i^*), \quad \phi_b = \frac{1}{\sqrt{2}}(\phi_i - \phi_i^*) \tag{10}$$

where ϕ_a and ϕ_b are mainly localized on atomic sites a and b, respectively, but they have small tails on a and b. Therefore, MNOs ϕ_a and ϕ_b are orthogonal as in the case of Anderson's theory of antiferromagnetism [43]. The magnetic molecular orbitals are rewritten by using MNO as

$$\psi_i^+ = \cos\left(\theta - \frac{\pi}{4}\right)\phi_a + \sin\left(\theta + \frac{\pi}{4}\right)\phi_b$$
$$\psi_i^- = \cos\left(\theta - \frac{\pi}{4}\right)\phi_b + \sin\left(\theta + \frac{\pi}{4}\right)\phi_a \quad (11)$$

The orbital overlap $T_i = \langle\psi^+|\psi^-\rangle$ is a measure of the spin delocalization, namely $T_i = 0$ for pure metal biradical and $T_i = 1$ for the closed-shell pair [47], and ${}^{LS}\langle s^2\rangle = \Sigma(1 - T_i)$ (i = magnetic orbitals)(see Eq. (6)).

Fig. 3 depicts the magnetic molecular orbitals for the up (α) and down (β) spins, which have been obtained by the mUS2WN method. The magnetic σ or δ orbitals were mainly localized on the left and right manganese atoms, respectively, though the delocalizations over the O_2 and $(NHCHCO_2)_4$ fragments were not negligible. On the other hand, the magnetic π orbitals exhibited significant delocalization over the whole molecular skeleton. The π delocalization was further enhanced under the UBLYP and UB3LYP approximations, in accordance with their overestimation of the $J_{ab}^{(3)}$ value. The situation is quite similar in the case of the H–He–H system in Table 1, and in the 2Fe–2S and 4Fe–4S systems [58,59]. Thus the well-refined DFT wavefunctions can be used for qualitative explanation of the superexchange interactions between manganese ions via oxygen anions. Very recently, the refined DFT schemes have been applied for other systems [65–67].

3. Spin alignments and spin tunneling in polynuclear magnetic clusters

The magnetization of the Mn_{12} cluster is highly anisotropic, and the magnetization relaxation time becomes very long at low temperature, showing the pronounced hysteresis. This behavior is not strictly analogous to that of a bulk ferromagnet, in which magnetization hysteresis results from the motion of domain walls. Tunneling across an anisotropy barrier is induced when an applied field makes one of the states resonant with the other as an excited level shown in Fig. 4(a-1).

Theoretical studies for the magnetic hysteresis have been carried out. Hernandez et al. [69] have measured the magnetization at low temperatures of tetragonal crystals of Mn_{12} acetate complex $[Mn_{12}O_{12}(CH_3COO)_{16}(H_2O)_4]$ and have pointed out the importance of thermally assisted resonant tunneling of the magnetization. They have calculated tunneling rates for different m values. According to their results, on resonance, the system is thermally activated within the metastable left well to an excited state near the top of the energy barrier, where it rapidly tunnels to the right well as shown in Fig. 5. Garanin et al. [70] have also reported thermally activated resonant magnetization tunneling in molecular magnets of Mn_{12} and other system by calculating the spin Hamiltonian of an isolated Mn_{12} molecule. De

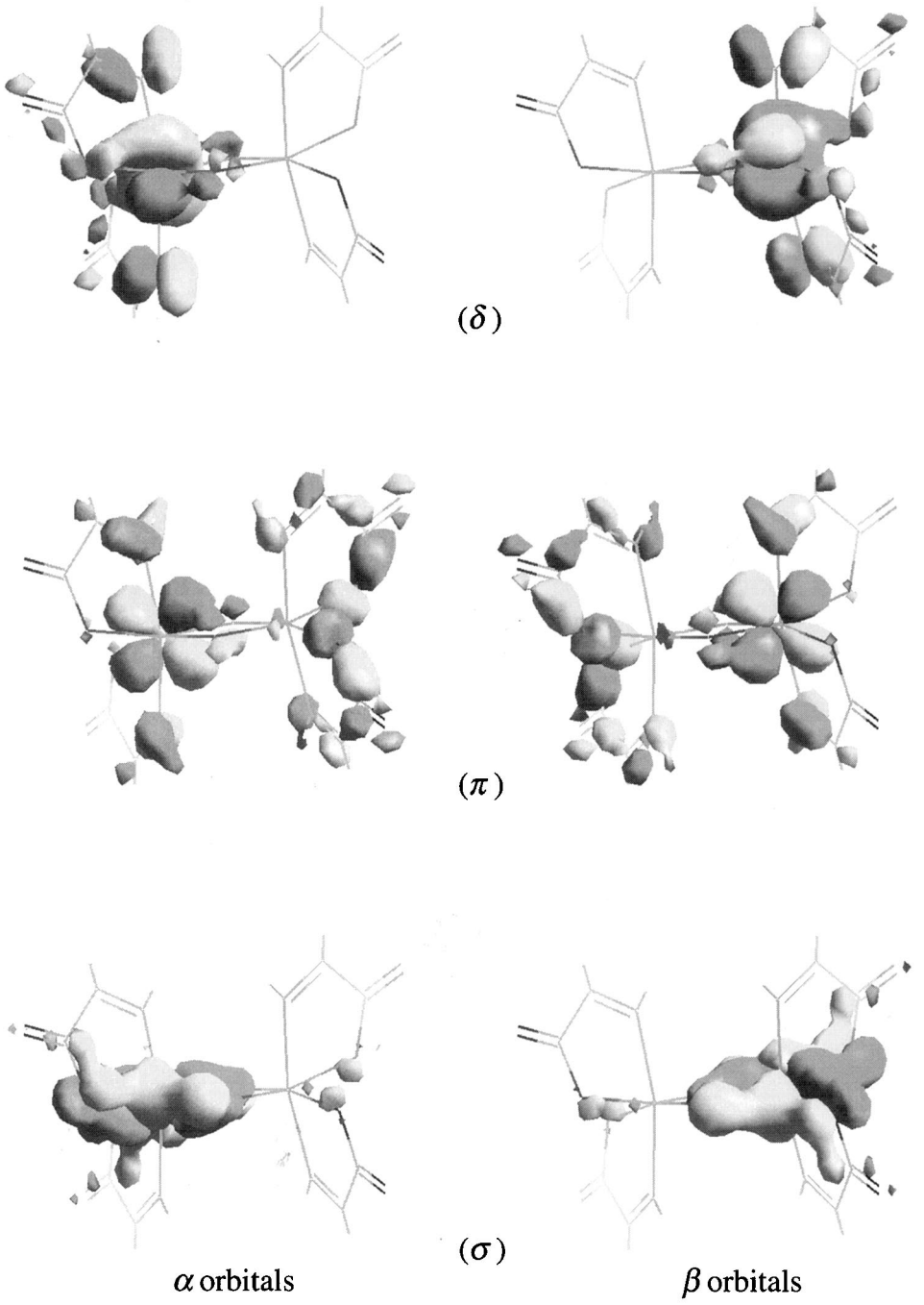

Fig. 3. Magnetic σ, π and δ molecular orbitals for the up (α) and down (β) spins obtained by the UB2LYP2 methods.

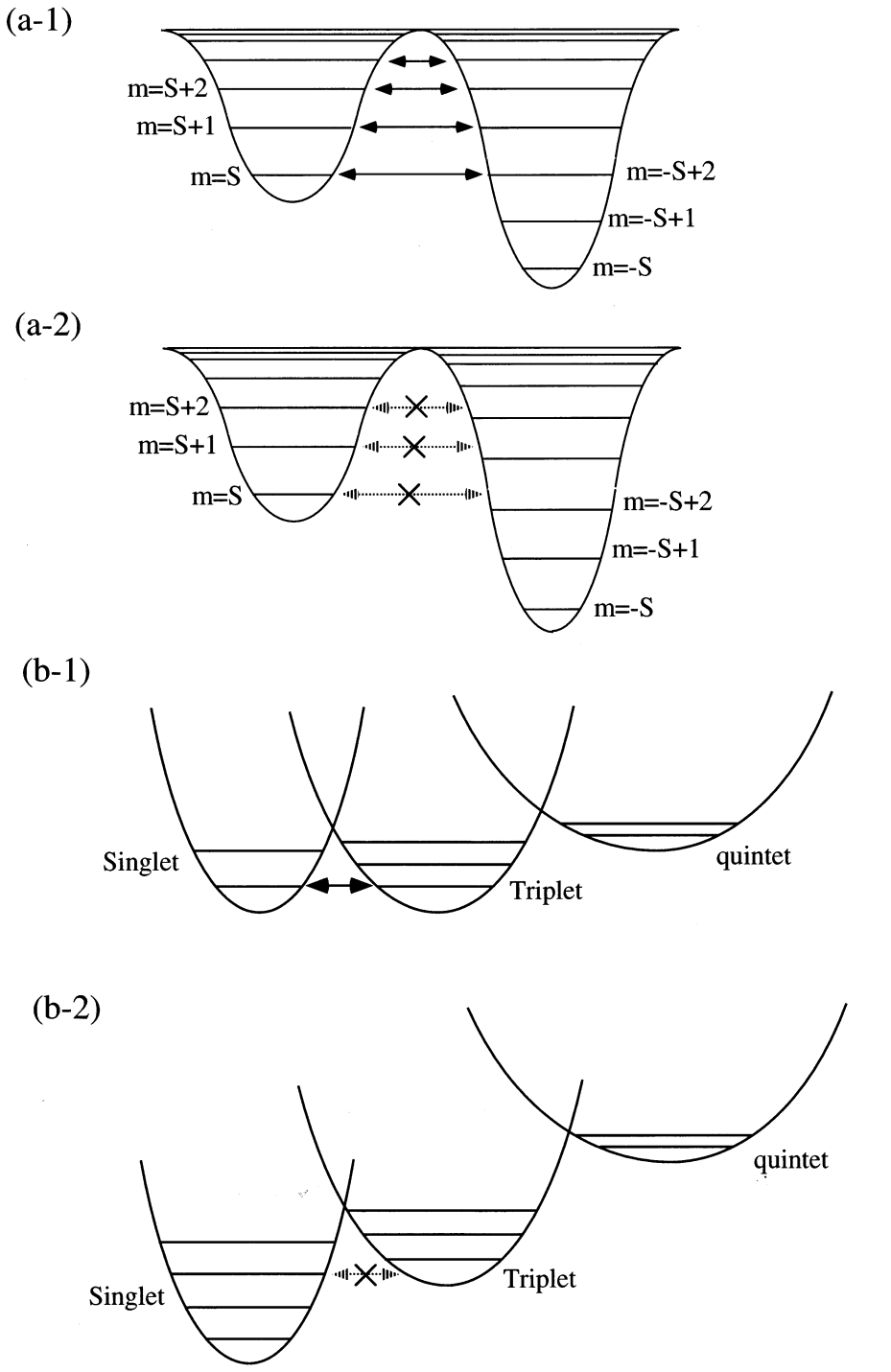

Fig. 4. Schematic diagrams of magnetic tunneling. (a-1) Tunneling for a system with a single collective spin degree of freedom. (a-2) Illustrates that tunneling vanishes. (b-1) Tunneling between singlet and triplet states. (b-2) Tunneling vanishes.

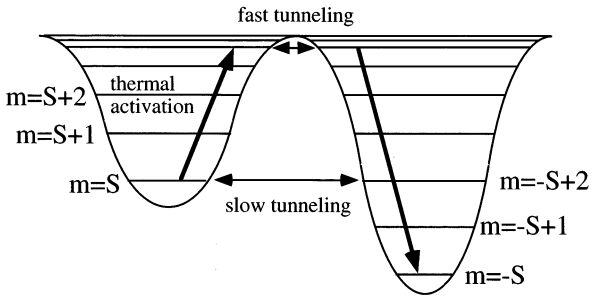

Fig. 5. Schematic diagram. Tunneling rate between excited states near the top of energy barrier is larger than that between ground states near the bottom.

Raedt et al. [71] have discussed quantum tunneling of the magnetization in relation to the sweep rate of the applied magnetic field. We have applied a quantum Monte Carlo method to the quantum magnetic tunneling problem [23].

In this and the follow sections, we discuss magnetic quantum tunneling [19–25] in several spin systems in relation to calculations of quantum tunneling rate, a classical spin structure of those spin systems and so on.

Two possible examples of magnetic quantum tunneling events are illustrated in Fig. 4. Fig. 4(a) shows a magnetic quantum tunneling of spin systems described by a single collective spin degree of freedom such as the Mn_{12} system. Fig. 4(b) indicates a magnetic quantum tunneling between singlet and triplet states such as spin level crossing by an external magnetic field. In this review, we focus on the former, though the latter is an interesting topic for the magnetic behavior of a ring structure comprised of metal ions with localized spin and large organic ligands such as the ferric wheel ($[Fe(OMe)_2(O_2CCH_2Cl)]_{10}$).

3.1. Spin alignments

Manganese oxide clusters with triangular, butterfly and cubic molecular structures have shown peculiar and complex magnetic behaviors [4,5]. We summarize in Fig. 6 several Mn clusters in relation to the network structure for the exchange interaction. Previously we determined the torsional angles of spins in iron–sulfur clusters on the basis of the classical Heisenberg model by using their observed effective exchange integrals [5]. It was found that these species exhibit general spin structures with two- and/or three-dimensional spill modulations. The magnetic double group theory [72] was applied to determine general spin orbitals for the 4Fe–4S cluster with tetrahedral symmetry [73]. In a previous paper [74], we calculated the torsional angles θ of spins using observed effective exchange integrals of typical manganese clusters shown in Fig. 6 in relation to symmetry and broken symmetry in molecular orbital (MO) theoretical descriptions. We gave an intuitive picture for antiferromagnetic spin coupling between the high-spin manganese ions in MnO systems.

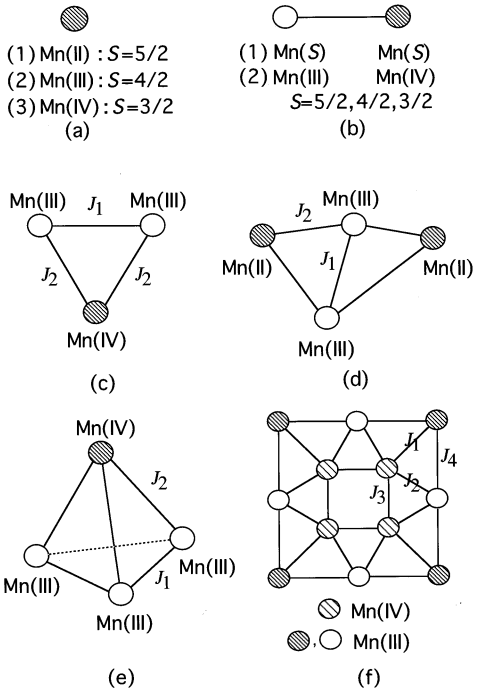

Fig. 6. Manganese clusters. (c) Triangular-type. (d) Butterfly-type. (e) Tetrahedral-type. (f) Mn_{12}.

To calculate the spin structure and the tunneling amplitude, we introduce here a coherent spin state, the so-called nonlinear σ model [75]. The tunneling amplitude is usually calculated by setting up a coherent spin state path integral and analytically continuing to imaginary time ($t \rightarrow -i\tau$); the leading contribution can be found using the method of steepest descent.

3.1.1. Nonlinear σ model

We briefly summarize the nonlinear σ model. The state of a spin at a given site is expressed with the following coherent basis [75]:

$$|\boldsymbol{\Omega}\rangle = |\theta, \phi\rangle = \mathrm{e}^{i\theta(\hat{S}_z - S)}\mathrm{e}^{-i\phi\hat{S}_y}|S\rangle \tag{12}$$

where $\boldsymbol{\Omega}$ is a vector on a unit sphere with spherical coordinates $(1, \theta, \phi)$, $0 \leq \theta \leq \pi$, $0 \leq \phi < 2\pi$, and $|S\rangle$ is the eigenstate of $\hat{S}_z$ with the largest possible eigenvalue S. The overlap of the coherent states is written as

$$\langle\boldsymbol{\Omega}|\boldsymbol{\Omega}'\rangle = \left[\frac{1}{2}(1 + \boldsymbol{\Omega}\cdot\boldsymbol{\Omega}')\right]^S \mathrm{e}^{-i\delta\phi S(1-\cos\theta)} \tag{13}$$

Note that $\delta\phi = \phi' - \phi$. The closure relation is constructed as

$$1 = \int \frac{d\boldsymbol{\Omega}}{4\pi}|\boldsymbol{\Omega}\rangle\langle\boldsymbol{\Omega}| \tag{14}$$

Therefore, we have the imaginary time transition amplitude:

$$\langle \boldsymbol{\Omega}(\beta)|\mathrm{e}^{-\beta H}|\boldsymbol{\Omega}(0)\rangle = \int_{\theta(0),\phi(0)}^{\theta(\beta),\phi(\beta)} D\Omega \exp\left[-\int_0^\beta \mathrm{d}\tau L\right] \tag{15}$$

where

$$D\Omega = \prod_\tau \mathrm{d}\phi_\tau \, \mathrm{d}\theta_\tau \sin\theta_\tau \tag{16}$$

β^{-1} is the temperature, and L is a Lagrangian:

$$L = iS\dot{\phi}(1-\cos\theta) + JS^2 \sum_{a,b} \boldsymbol{\Omega}_a \cdot \boldsymbol{\Omega}_b \tag{17}$$

and we use the Heisenberg Hamiltonian:

$$H = J \sum_{a,b} \boldsymbol{S}_a \cdot \boldsymbol{S}_b \tag{18}$$

The first term of Eq. (17) defines the Wess–Zumino term [21,22,75] of the topological one. The dot on $\dot{\phi}$ means ∂_τ. The phase of the tunneling amplitude depends on a topological phase, the so-called Berry phase or Wess–Zumino phase.

3.1.2. Classical spin structure

Using the coherent state of Eq. (12), we can obtain the classical spin picture [11,12,74] as shown in Fig. 7(a). Here, we calculate the potential surface of the ground state of a manganese oxide cluster. As an example, the butterfly-type Mn_4 cluster as shown in Fig. 8(a) is considered. We consider two spins ($S_1 = S_2 = 4/2$) of two Mn(III) ions in the ground state. The Hamiltonian for the butterfly-type system is written as

$$H = J_1 \boldsymbol{S}_1 \cdot \boldsymbol{S}_2 + 2J_2 \boldsymbol{S}_1 \cdot \boldsymbol{Z} + 2J_2 \boldsymbol{S}_2 \cdot \boldsymbol{Z} - \boldsymbol{B} \cdot \boldsymbol{S}_1 - \boldsymbol{B} \cdot \boldsymbol{S}_2 - 2\boldsymbol{B} \cdot \boldsymbol{Z} \tag{19}$$

where $\boldsymbol{Z}$ is defined by the Mn(II) spins and $\boldsymbol{B}$ is the intensity of the external magnetic field. Setting up a coordinate as shown in Fig. 7(b) and performing the variational energy calculation of $\langle \boldsymbol{\Omega}|H|\boldsymbol{\Omega}\rangle$ [26], we obtain the ground-state energy E involving only a single (collective) spin degree of freedom with an effective spin of $2S$ for the ground state:

$$E = 2S^2 J_1 \left(\cos\theta + \frac{2J_2 S' - B}{2J_1 S}\right)^2 - J_1 S^2 - \frac{(2J_2 S' - B)^2}{2J_1} - 2BS' \tag{20}$$

The spin structure for the ground state is illustrated in Fig. 8(b). The expectation value for each Mn cluster system shown in Fig. 6 is summarized in Table 3.

For this Mn_4 cluster, we take $[Mn_2^{II}Mn_2^{III}O_2(O_2CMe)_6(bipy)_2]$ [76]. According to experimental results [76], the effective exchange integrals of J_1 and J_2 are 3.12 and 1.97 cm^{-1}, respectively. Fig. 9(a) shows the potential energy surface for this manganese cluster without external magnetic field. From Eq. (20) we find the ground-state energy of 34.75×10^{-4} eV when

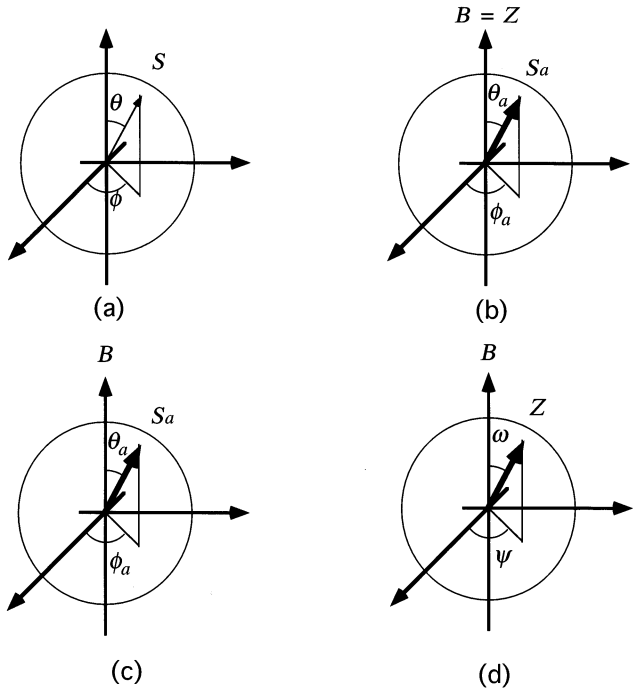

Fig. 7. (a) Classical spin picture. (b) The spin $\boldsymbol{S}_a$ and the external magnetic field $\boldsymbol{B}$ ($\boldsymbol{Z}=\boldsymbol{B}$). (c) and (d) Spin picture of $\boldsymbol{S}_a$ and $\boldsymbol{Z}$. The case of $\boldsymbol{Z}\neq\boldsymbol{B}$.

Table 3
Effective Lagrangians for Mn clusters

System	Effective Lagrangian
A	$L=-iZ\dot{\phi}(1-\cos\omega)+BZ\cos\omega$
B	$L=-iS\dot{\phi}(1-\cos\theta)-(JZ-B)S\cos\theta+BZ$
C	$L=-i2S\dot{\phi}(1-\cos\theta)-J_1 2S^2\left(\cos\theta+\frac{J_2Z-B}{2J_1S}\right)^2+J_1S^2+\frac{(J_2Z-B)^2}{2J_1}+BZ$
D	$L=-i2S\dot{\phi}(1-\cos\theta)-J_1 2S^2\left(\cos\theta+\frac{2J_2Z-B}{2J_1S}\right)^2+J_1S^2+\frac{(2J_2Z-B)^2}{2J_1}+2BZ$
E	$L=-i3S\dot{\phi}(1-\cos\theta)-J_1 6S^2\left(\cos\theta+\frac{J_2Z-B}{4J_1S}\right)^2+3J_2S^2+\frac{3(J_1Z-B)^2}{8J_2}+BZ$
F	$L=-i4S\dot{\phi}(1-\cos\theta)-8J_3S^2\left(\cos\theta+\frac{(2J_2+J_1)Z-2B}{4J_3S}\right)^2-8J_4Z^2+8BZ+4J_3S^2+\frac{[(2J_2+J_1)Z-2B]^2}{8J_3}$

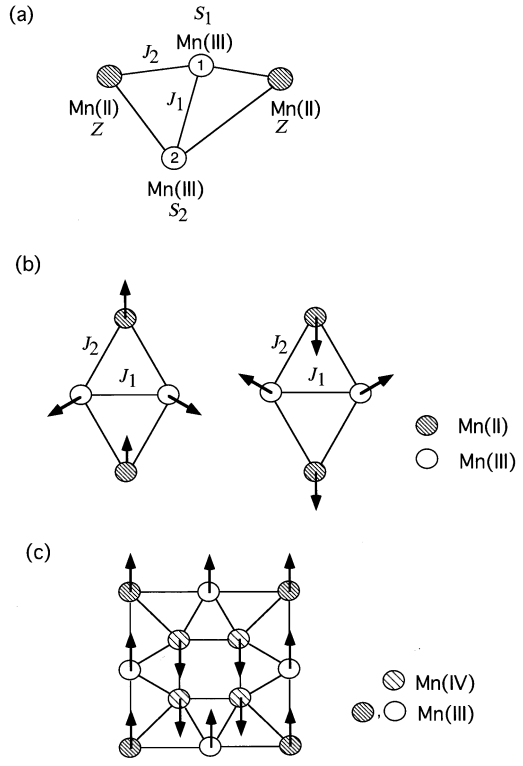

Fig. 8. (a) Butterfly-type Mn_4 cluster. (b) Spin structure of the ground state of butterfly-type Mn cluster. (c) Ground state of Mn_{12}.

$$\cos\theta = -\frac{J_2 S'}{J_1 S} = -0.789, \quad \theta = 142.09 \tag{21}$$

This means that the classical spin structure of the ground state is helical, as shown in Fig. 8(b).

For the Mn_{12} cluster shown in Fig. 6(f), the effective exchange integrals have been experimentally investigated [15] ($J_1 = 150$, $J_2 = 60$, $J_3 = 57.5$, $J_4 = 30$ (cm^{-1})). Using the results from Table 3, we find that $\theta = \pi$ as shown in Fig. 8(c) in the absence of the external field. Therefore, the classical spin structure becomes axial.

3.1.3. Effective Lagrangian for one ground state

The tunneling amplitude is usually calculated by setting up a coherent-spin-state path integral and analytically continuing to imaginary time ($t \to -i\tau$); the leading contribution can be found using the method of steepest descent. The phase of the tunneling amplitude depends on a topological phase, the so-called Berry or Wess–Zumino phase.

Magnetic quantum tunneling between ground states is shown for the butterfly-type Mn cluster in Fig. 8(b). In Fig. 7(c) and (d), it is shown from the Lagrangian that the

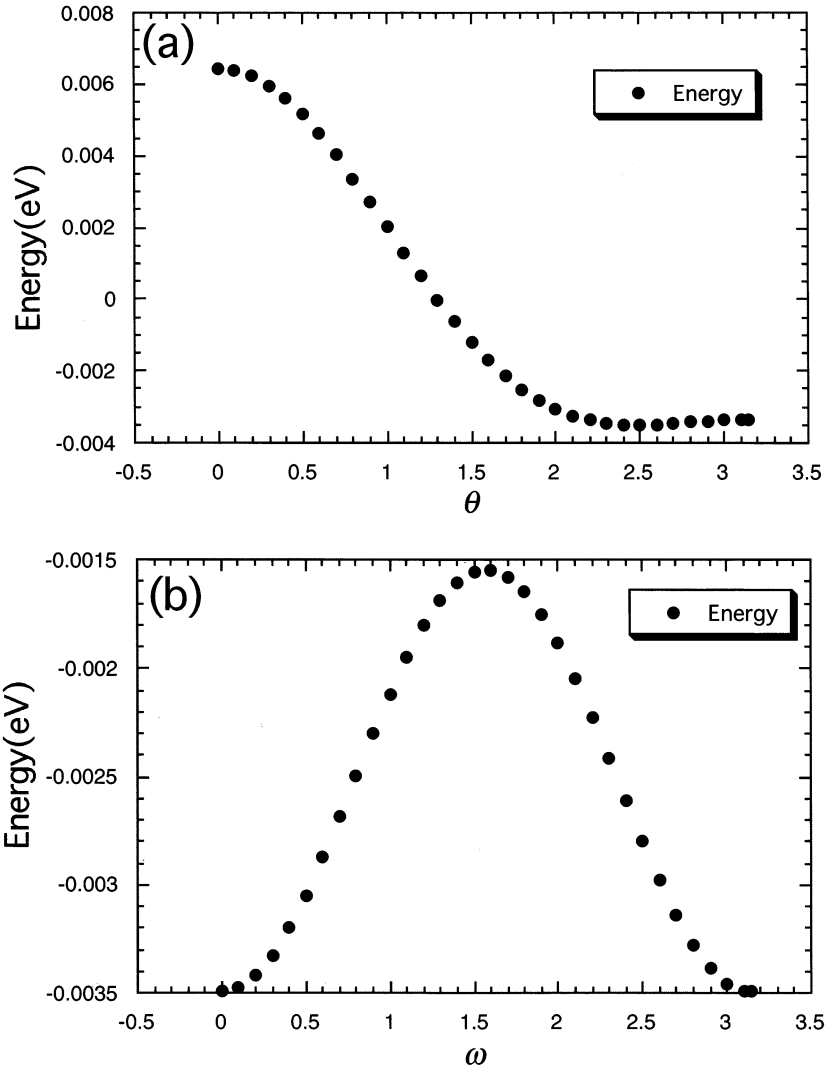

Fig. 9. Energy potential surface of butterfly-type $[Mn^{II}_2Mn^{III}_2O_2(O_2CMe)_6(bipy)_2]$. (a) Energy vs. θ. (b) Energy vs. ω.

tunneling problem of the butterfly-type Mn_4 cluster can be mapped onto a simple model problem defined by an effective Lagrangian

$$L_{\text{eff}} = -iS_{\text{eff}}\dot{\psi}(1-\cos\omega) + \frac{2J_2^2S'^2}{J_1}\left[\cos\omega - \frac{B}{2J_2S'}\left(1-\frac{J_1}{J_2}\right)\right]^2 + J_1S^2 - \frac{B^2}{J_1} - \frac{B^2}{2J_1}\left(1-\frac{J_1}{J_2}\right)^2 \quad (22)$$

with an effective spin of S_{eff}, where S_{eff} is $2S$ in this case, though the total spin vanishes. The ground state is shown to be the same as that derived from Eq. (20) when ω is 0 or π. The double-well potential surface obtained from Eq. (22) is also shown in Fig. 9(b).

3.1.4. Simple model with anisotropic energy

A simple model for a single molecular system with an anisotropic energy as the Mn_{12} cluster and the butterfly-type Mn cluster is represented as a Hamiltonian:

$$H = DS_z^2 - \boldsymbol{B} \cdot \boldsymbol{S} \tag{23}$$

where D indicates an anisotropic energy. Using the coherent-spin-state of Eq. (12), the expectation value is written as

$$\langle \boldsymbol{\Omega}|H|\boldsymbol{\Omega}\rangle = -DS^2\left(\cos\theta + \frac{B}{2DS}\right)^2 + \frac{B^2}{4D} \tag{24}$$

In the absence of an external magnetic field, we get the double-well potential surface giving by $-DS^2\cos^2\theta$.

3.2. Spin tunneling probability

3.2.1. Simple model

We calculate the magnetic quantum tunneling rate from 0 to π in the case of the simple model with an anisotropic energy. In this model the expectation value, becomes the ground-state energy of $-DS^2$ when $\theta = 0$ or π. Therefore, we calculate the imaginary time transition amplitude $\langle\pi|e^{-\beta H}|0\rangle$, where $\langle\pi| = \langle\theta = \pi, \phi(\beta)|$, $|0\rangle = |\theta = 0, \phi(0)\rangle$, and H means the Hamiltonian of Eq. (23).

The imaginary time tunneling amplitude from 0 to π can usually be calculated by using an instanton approximation in order to obtain the tunneling rate [74]. Here, however, we calculate it by summing contributions from all paths [77,78] according to Feynman's original idea. According to the procedure used in previous papers [77,78], we start by dividing $e^{-\beta H}$ into n factors, and by using a closure relation of Eq. (14), we have

$$\langle\pi|\mathrm{e}^{-\beta H}|0\rangle = \int \prod_{l=1}^{n-1} \frac{\mathrm{d}\boldsymbol{\Omega}(l)}{4\pi} \prod_{k=0}^{n-1} \langle \boldsymbol{\Omega}(k+1)|\mathrm{e}^{-\tau H}|\boldsymbol{\Omega}(k)\rangle \tag{25}$$

where $\tau = \beta/n$, $\langle\boldsymbol{\Omega}(n)| = \langle\pi,0|$, and $|\boldsymbol{\Omega}(0)\rangle = |0,0\rangle$. From the matrix element on the right-hand side of Eq. (25), the contribution from a path with a transition from $\omega(\tau') = 0$ to $\omega(\tau' + \delta\tau) = \pi$ is approximately given by

$$\mathrm{e}^{-\beta\epsilon_0}\mathrm{e}^{-\bar{\epsilon}}[1 - \tau\delta\epsilon] \tag{26}$$

where

$$\delta\epsilon = -\frac{DS^2}{2}, \quad \bar{\epsilon} = -\epsilon_0 + \frac{1}{\pi}\int_0^{\pi} \mathrm{d}\omega(-DS^2\cos^2\omega) = \frac{DS^2}{2} \tag{27}$$

and ϵ_0 is the ground-state energy of $-DS^2$. The first term in Eq. (26), which arises from the overlap of the coherent state of Eq. (14), yields infinite contributions to

the imaginary time transition amplitude. Because we focus our attention on the tunneling rate, we consider only the second term in Eq. (26) to obtain the tunneling amplitude [79], namely, the contribution f_1 without the zero-mode is treated. After the theoretical derivation [77], we have

$$\langle \pi | e^{-\beta H_{\text{eff}}} | 0 \rangle = e^{-\beta \epsilon_0} \sinh(-\beta e^{-\bar{\epsilon}} \delta\epsilon) \tag{28}$$

Therefore, the magnetic quantum tunneling rate (energy level splitting) P, defined by the energy gap occurring from the tunneling effects, from 0 to π in the potential surface is derived from Eq. (28) as

$$P = 2e^{-\bar{\epsilon}}(-\delta\epsilon) = DS^2 e^{-DS^2/2} \tag{29}$$

The results suggest that the tunneling rate reaches a maximum, when $D = 2/S^2$.

3.2.2. Mn_4 cluster

We calculate the magnetic quantum tunneling rate from 0 to π in the effective potential surface derived from Eq. (22), as shown in Fig. 9(b), for the butterfly-type Mn cluster without an external magnetic field. For simplicity, we consider a model for the effective Lagrangian of Eq. (22) and introduce a coherent state $|\Xi\rangle$ and an effective Hamiltonian H_{eff}, which gives the expectation value:

$$E = \langle \Xi | H_{\text{eff}} | \Xi \rangle = -a \cos^2 \omega + b \tag{30}$$

where a and b are constants. Note that this model describes the magnetic behavior of the butterfly-type system when $a = 2J_2^2 S'^2/J_1$ and $b = -J_1 S^2$ (see Eq. (22)). In this model the expectation value becomes the ground-state energy of $-a + b$ when $\omega = 0$ or π.

In a similar procedure, we obtain the general expression of the imaginary time transition amplitude as

$$\langle \pi | e^{-\beta H_{\text{eff}}} | 0 \rangle = e^{-\beta \epsilon_0} \sinh(-\beta e^{-\bar{\epsilon}} \delta\epsilon) \tag{31}$$

where

$$\delta\epsilon = -\frac{a}{2}, \quad \bar{\epsilon} = -\epsilon_0 + \frac{1}{\pi} \int_0^{\pi} d\omega(-a \cos^2 \omega + b) = \frac{a}{2} \tag{32}$$

and ϵ_0 is the ground-state energy of $-a + b$. Therefore, the magnetic quantum tunneling rate is derived from Eq. (31) as

$$P = 2e^{-\bar{\epsilon}}(-\delta\epsilon) = ae^{-a/2} \tag{33}$$

From Eq. (33) and the constants in Eq. (30) for the butterfly-type Mn cluster, the magnetic quantum tunneling rate with the effective potential in Eq. (22) shown in Fig. 6(b) is given by

$$P = \frac{4J_2^2 S'^2}{J_1} e^{-J_2^2 S'^2/J_1} \tag{34}$$

The tunneling rates for other cases are similarly derived from the Lagrangians in Table 3.

4. Macroscopic quantum tunneling of spin in a mesoscopic system

4.1. Quantum spin tunneling in spin–lattice

Recently, Fujii et al. [80] have reported that the nuclear spin–latticie relaxation times T_1 of ^1H in organic radical salts m-MPYNN$^+\cdot$X$^-\cdot$1/3(acetone)(X = ClO_4, BF_4) were measured at ultra-low temperatures. They suggested that temperature-independent magnetic fluctuation is caused by the frustration effect associated with quantum spin tunneling in the Kagomé antiferromagnet of the $S = 1$ dimer.

Some molecular cluster magnets [81,82] have a ring structure such as the ferric wheel ($[Fe(OMe)_2(O_2CCH_2Cl)]_{10}$), which consists of an Fe_{10} ring bridged by oxygen atoms and large organic ligands. The Fe_{10} ring is a paramagnet, and its ground state is nonmagnetic rather than antiferromagnetic. It was experimentally found that the magnetization increases in a stepwise manner at very low temperature.

Here, we discuss quantum spin tunneling in the Kagomé lattice and a ring-spin system in relation to an integer or half-integer spin and the topological term.

4.1.1. Kagomé lattice

von Delft et al. [24] have studied the total tunneling amplitude in tunneling between different ground-state configurations of the Kagomé lattice quantum Heisenberg antiferromagnet by using a coherent spin-state path integral. As they have shown, the total tunneling amplitude becomes zero in the half-integer spin, because the topological phase factors, the so called Berry or Wess–Zumino phase, of the corresponding tunneling amplitudes can lead to destructive interference between different paths.

Spin tunneling in a spin–lattice is discussed in relation to the half-integer spin and the topological spin phase. As an example, we consider a two-dimensional quantum Heisenberg nearest-neighbor antiferromagnet on a Kagomé lattice as shown in Fig. 10(a). The Hamiltonian is written as

$$H = J \sum_{\langle a,b \rangle} \boldsymbol{S}_a \cdot \boldsymbol{S}_b \quad (J > 0) \tag{35}$$

Note that using the coherent spin state of Eq. (12), we get the classical spin picture. Any configuration in which the spins on each triangle minimize their energy by assuming a coplanar configuration with relative angles of 120° as shown in Fig. 10(b) is a classical ground state configuration [11,73]. There are, therefore, macroscopically many degenerate classical ground states.

As the simplest example of a tunneling event on the Kagomé lattice, we consider the six spins of a hexagon in one maximally coplanar ground state, $|i\rangle$, rotate synchronously by 180° around the z axis, to end up at another maximally coplanar ground state, $|f\rangle$, while all other spins remain fixed (see Fig. 10(b)). In the framework of this assumption, the Hamiltonian of Eq. (35) is rewritten as

$$H = J \sum_{a=1}^{6} \left[\boldsymbol{S}_a \cdot \boldsymbol{S}_{a+1} + \boldsymbol{S}_a \cdot \boldsymbol{Z} + \boldsymbol{S}_{a+1} \cdot \boldsymbol{Z} + \frac{3}{2} \right] + J_b f(\phi_{av}) \tag{36}$$

where $J_b f(\phi)$ indicates a coplanarity barrier, and $f(\phi)$ is the barrier shape function obeying $f(\phi) = f(-\phi)$. The index j is defined modulo 6, and $\phi_{av} = 1/6\Sigma_{a=1}^{6}(\phi_j - \phi_j(0))$

In a similar way, using the coherent state, we obtain an effective Lagrangian

$$L = i6S\dot{\phi}(1-\cos\theta) + 12S^2J\left(\cos\theta + \frac{1}{2}\right)^2 + J_b \sin^2\phi \tag{37}$$

The effective Lagrangian involves only a single (collective) spin degree of freedom with an effective spin of $6S$; $S_{\text{eff}} = 6S$.

From the effective potential on the right-hand side of Eq. (37), when $\cos\theta$ is $-1/2$, and ϕ is 0 or π, we obtain the ground state. Then, we find that the expectation value of the potential part in the ground state becomes 0. Therefore, we calculate a imaginary time transition amplitude from ϕ of 0 to π, when $\cos\theta = -1/2$.

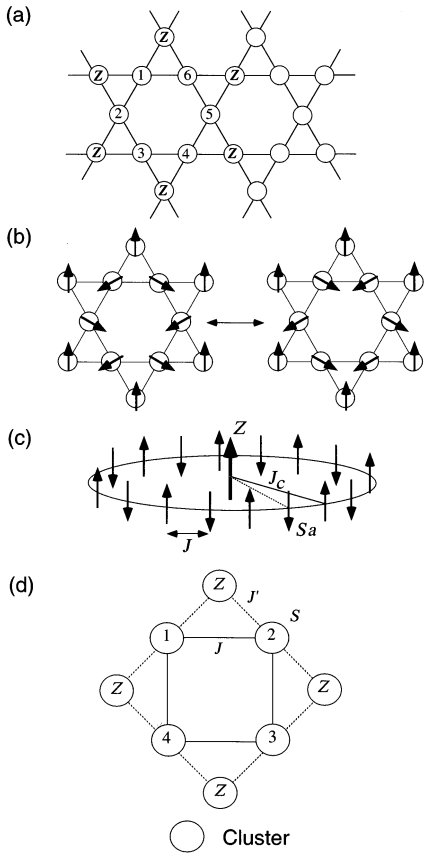

Fig. 10. (a) Kagomé lattice. (b) Ground state of one hexagon. (c) One-dimensional antiferromagnetic ring. (d) A cluster of clusters.

According to the similar procedure for calculation of the imaginary time transition amplitude, we get the transition amplitude from 0 to π:

$$\langle \pi | e^{-\beta H} | 0 \rangle = e^{-\beta \epsilon_0} \sinh(-2\beta \cos \pi S_{\text{eff}} e^{-\bar{\epsilon}} \delta\epsilon) \tag{38}$$

where

$$\epsilon_0 = J_b, \quad \bar{\epsilon} = -\frac{J_b}{2}, \quad \delta\epsilon = \frac{J_b}{2} \tag{39}$$

From Eq. (38), the magnetic quantum tunneling rate with the effective potential in Eq. (37) is given by

$$P = 2J_b e^{-J_b/2} |\cos(\pi S_{\text{eff}})| \tag{40}$$

From Eq. (40), we find that the tunneling rate vanishes for a half-integer spin system. When the effective spin of $6S$ is an integer, tunneling rate becomes $2J_b e^{-J_b/2}$.

4.1.2. One-dimensional antiferromagnetic ring

Loss et al. [25] have also suggested that quantum tunneling of magnetization in one-dimensional antiferromagnet ring vanishes for magnetic particles with a half-integer spin but is finite for an integer spin by a coherent state path integral calculation.

We consider a one-dimensional antiferromagnetic ring with N spins $\boldsymbol{S}_a$, (spin magnitude S) and periodic boundary conditions; all the spins $\boldsymbol{S}$ are coupled to a central excess spin $\boldsymbol{Z}$ with coupling constant $J_c^a = (-1)^a J_c$, as shown in Fig. 10(c). Thus the central spin will prefer to remain aligned with the Néel vector of the spins on the ring. The Hamiltonian of the system may be written as

$$H = \sum_{a=1}^{N} [J\boldsymbol{S}_a \cdot \boldsymbol{S}_{a+1} + J_c^a \boldsymbol{S}_a \cdot \boldsymbol{Z} + H(\boldsymbol{S}_a)] \tag{41}$$

where N is even, and the last term on the right-hand side of Eq. (41) is the anisotropy Hamiltonian:

$$H(\boldsymbol{S}_a) = K_z^a (S_a)_z^2 + K_y^a (S_a)_y^2 \tag{42}$$

with $K_z^a > K_y^a > 0$.

Using the coherent state of Eq. (12), the expectation value E becomes

$$E = N(2J + K_z - K_y \sin^2 \phi) S^2 \cos^2 \theta + NJ_c SZ \cos \theta - NJS^2 + NK_y S^2 \sin^2 \phi \tag{43}$$

where $K_y^a = K_y$, $K_z^a = K_z$, and $J_c^a = J_c$. When we consider a condition which is $K_z \gg K_y > 0$, the minimum expectation value $E_{\min}$, approximately becomes

$$E_{\min} \approx -NJS^2 - \frac{NJ_c^2 Z^2}{8J + 4K_z} + NK_y S^2 \sin^2 \phi \tag{44}$$

with

$$\cos\theta_{\min} \approx -\frac{J_c Z}{(4J+2K_z)S} \tag{45}$$

In a similar way, we can also obtain an effective Lagrangian of the ground state for Eq. (44).

$$L = iZ\dot{\phi}(1-\cos\theta_{\min}) + NK_y S^2 \sin^2\phi - NJS^2 - \frac{NJ_c^2 Z^2}{8J+4K_z} \tag{46}$$

Note that the effective spin on the right-hand side of Eq. (46) becomes the central excess spin. The magnetic quantum tunneling rate with the effective potential in Eq. (44) is given by

$$P = 2NK_y S^2 \mathrm{e}^{-NK_y S^2/2}\left|\cos(\pi Z)\right| \tag{47}$$

It is found that when the central excess spin is a half-interger spin, the tunneling rate vanishes.

4.2. MQT in a cluster of clusters

Here, we consider a cluster, which consists of clusters with anisotropic energy, as shown in Fig. 10(d) and suppose that the Hamiltonian of each cluster in the cluster is represented by the simple model of Eq. (23):

$$H_a = -D(S_a)_z^2 - \boldsymbol{B}\cdot\boldsymbol{S}_a \tag{48}$$

where D indicates the anisotropic energy, and $\boldsymbol{B}$ is the external magnetic field. The total Hamiltonian of the system shown in Fig. 10(d) may be written as

$$H = \sum_{a=1}^{4}\left[J\boldsymbol{S}_a\cdot\boldsymbol{S}_{a+1} + J'\boldsymbol{S}_a\cdot\boldsymbol{S}_z + J'\boldsymbol{S}_{a+1}\cdot\boldsymbol{S}_z + H_a + H_z\right] \tag{49}$$

Note that the anisotropic energy D is independent of the interactions between clusters in the cluster and the external magnetic field.

Using the coherent state of Eq. (12), we obtain the effective Lagrangian of the ground state for the three cases:

$$L = i4S\dot{\phi}(1-\cos\theta) \mp 4(D-2J)S^2\left(\cos\theta \mp \frac{2J'S-B}{2(D-2J)S}\right)^2 \pm \frac{(2J'S-B)^2}{D-2J} - 4(DS+JS+B)S \quad (D-2J \gtrless 0) \tag{50}$$

$$L = i4S\dot{\phi}(1-\cos\theta) - (2J'S-B)S\cos\theta - (3JS+B)S \quad (D-2J=0) \tag{51}$$

From Eqs. (50) and (51), it is found that when $D-2J$ is positive, the spin structure becomes axial, and when it is negative, it is helical as shown in Fig. 11(a). When the spin structure is axial, we can obtain a diagram of the magnetization of the ground state as shown in Fig. 11(b). In the case of the helical spin structure, when the system have a coplanarity barrier as the Kagomé lattice, we can expect the tunneling event between maximally coplanar ground states.

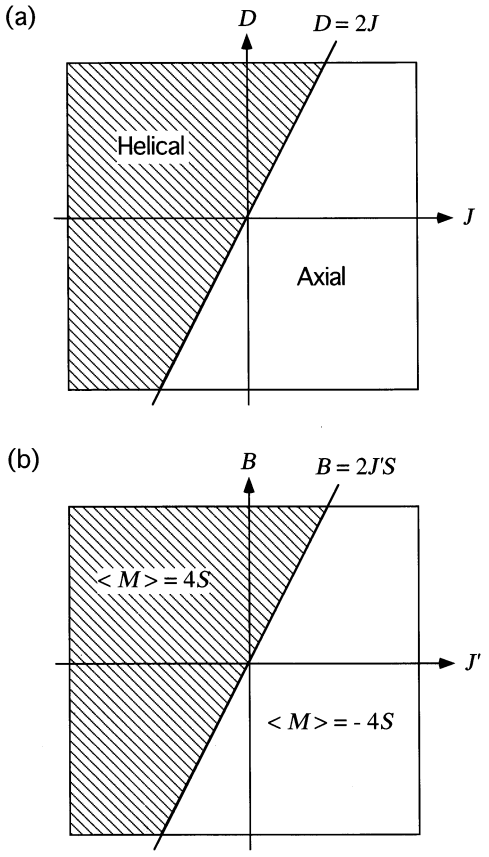

Fig. 11. (a) Phase diagram of the spin structure. (b) Phase diagram of the magnetization in an axial spin structure.

5. Concluding remarks

5.1. Theoretical approaches to molecular magnetism

Fig. 12 illustrates the theoretical approach to molecular magnetism employed by our group. We first perform ab initio molecular orbital calculations on binuclear transition metal complexes under the spin-unrestricted Hartree–Fock (UHF), spin-polarized density functional (DFT), and UHF plus DFT hybrid approximations. The effective exchange integrals (J_{eff}) between spins in the complexes are obtained by the total energies as shown in Eq. (6). The effective spin Hamiltonians, Heisenberg models, for polynuclear transition metal complexes are constructed assuming effective exchange interactions between nearest neighbor spins with neglect of multi-center interactions. The effective Lagrangians are derived for several typical clusters using these Heisenberg model. The spin structures of the

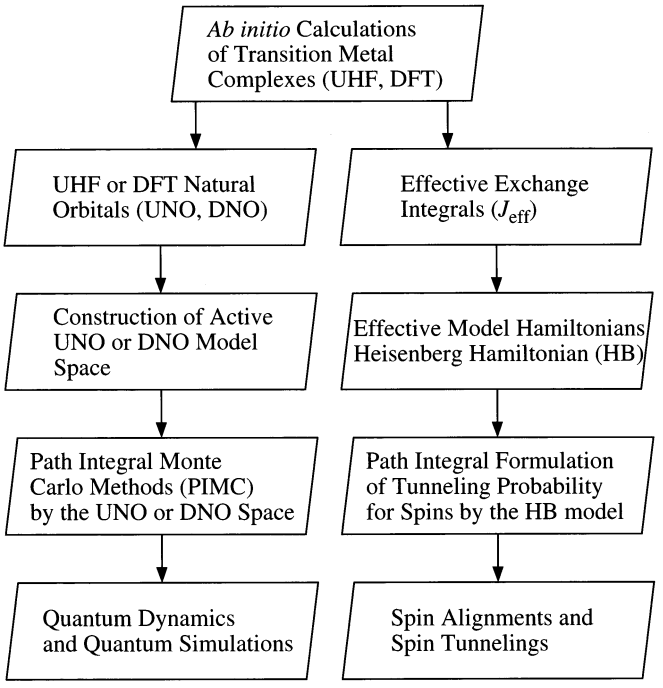

Fig. 12. Theoretical approaches to molecular magnetism.

complexes are elucidated based on these simplified models. The path integral formulations of tunneling probabilities are carried out based on the spin coherent representation, the so-called nonlinear σ model. [75].

The approximate natural orbitals (UNO or DNO) and their occupation numbers are determined by diagonalizing the first-order density matrices of the UHF or DFT solutions [62]. Active UNO and DNO spaces are constructed considering the occupation numbers. The CASCI by the use of the active UNO or DNO spaces are performed to elucidate excited states of the clusters [63] using HONDO-95 [83] and GAUSSIAN-94 [84] program packages. The path integral Monte Carlo (PIMC) methods [85–90] is also applied to calculations of the partition function and magnetization. The quantum dynamics and simulations under external magnetic field are carried out for magnetic clusters by the PIMC method. The computational schemes in Fig. 12 would be applicable to magnetic clusters in general.

5.2. Magnetic quantum tunneling

We have investigated the magnetic quantum tunneling of Mn clusters in relation to the molecular structure and integer or half-integer spins. General expressions of the imaginary time transition amplitude are derived by using the path integral of the nonlinear σ model [26]. We also present an expression for the magnetic

quantum tunneling rate for the Mn cluster having the butterfly structure. A similar procedure can be applied for calculation of the quantum tunneling rate for the Mn_{12} cluster. The spin structure and the magnetization of a cluster of clusters which has an anisotropic energy are also theoretically investigated. In such a cluster, the interaction between clusters in the cluster is important for constructing the spin helical or axial structure. The magnetization of two models, which correspond to a one-dimensional ring magnet and a ring system with an excess spin, are calculated by the Monte Carlo method. The results suggest that the former obeys the Landé interval rule, and that the latter does not. The magnetic behavior may be more interesting from the viewpoint of the molecular magnet. Recently, Sessoli et al. [91,92] made a comparison of the dynamic magnetic behavior of two octanuclear clusters of transition metal ions differing only in crystal packing, and the hysteresis loops for Mn_{12}Ac and reduced half-integer spin analogue. They suggested from experiments on spin relaxation that the magnetic tunneling rate of half-integer spin systems vanishes. Our results also predict that the tunneling rate vanishes for a half-integer spin cluster system in agreement with their experiments [91,92].

5.3. Molecular magnetic devices

Recently many theoretical and experimental studies have been carried out for new models of computation; DNA, quantum and reversible computers. The single molecule magnet such as the Mn_{12}–Ac complex [14–18] has received much interest in relation to quantum computing (QC), which utilizes the entanglement and superposition principle in quantum mechanics for parallel computation [93–98]. Quantum mechanical computing has already been carried out using NMR quantum computing, since the decoherence effect was not serious in the nuclear spin systems [99].

We similarly expect quantum computing in terms of various single molecular magnets by the control of spins with an external magnetic field or with photon modes will be performed in the future, since EPR can read the out-put information. However, there are several problems to overcome such as quantum relaxation, decoherence, etc, before the application of the single molecule magnet in molecular devices for the quantum computer can be realized. Apparently much experimental and theoretical effort is necessary to overcome such problems. The quantum simulations of the magnetic-field induced spin transitions [87] and nonlinear optical responses [100] are our first step toward such a goal.

5.4. Reactivity of manganese–oxygen bonds

In this review we did not touch on the chemical reactions of manganese oxides with water, which are of great interest in relation to the O_2-evolving complex in photosystem II. The manganese complex $[Mn_2^{IV}O_2(NHCHCO_2)_4]$ studied here would be a possible model for the active manganese site for the formation of molecular oxygen from water. According to recent experiments by Limburg et al. [101] and others, the manganese-oxo bonds may be formed via several reactions of

the complex as shown in Fig. 13. They concluded that the MN–O site generated first, abstracts a proton or hydrogen atom from water, and O_2 is formed from successive reactions. As shown previously [52], the manganese–oxygen bonds are labile, giving rise to cationic, radical and anionic oxygen sites, depending on the oxidation state of manganese ion, ligands and other factors such as hydrogen bonds as illustrated in Fig. 13. Therefore electrophilic, radical and nucleophilic reactions of Mn–O with H_2O are theoretically conceivable because of the complex nature of the dπ–pπ bond. For example, the Mn–O π bond in high valent Mn complexes exhibits significant biradical character (↑ · Mn–O · ↓) [52], which is responsible for radical abstraction of hydrogen from substrates. Therefore hydrogen abstraction from water is not surprising at least from our theoretical viewpoint [52]. The

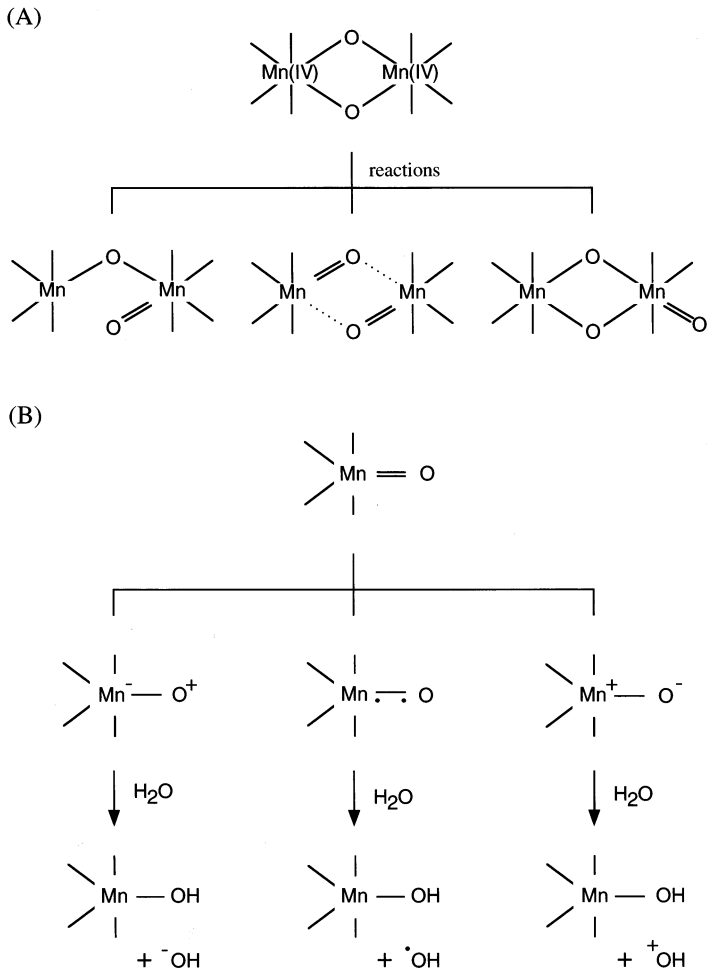

Fig. 13. (A) Generation of manganese-oxo bonds via chemical reactions and (B) three different reaction modes of the Mn–O bond with water.

modified hybrid DFT methods [65–67] would be particularly useful for MO theoretical investigations of these reactions. In fact, several groups have already initiated such theoretical studies [102,103]. Theoretical studies on possible reaction paths under several different environmental conditions are also in progress in our laboratory [104].

Acknowledgements

This work was supported by Grants-in-Aid for Scientific Research on Priority Areas (nos. 10132241, 10149105 and 10146102) from the Ministry of Education, Science, Sports and Culture, Government of Japan.

References

[1] J.K. McCuster, E.A. Schmitt, D.N. Hendrickson, in: D. Gatteschi, et al. (Eds.), Magnetic Molecular Materials, Kluwer, Dordrecht, 1991.
[2] O. Kahn, Molecular Magnetism, VCH, New York, 1993.
[3] J.S. Miller, A. Epstein, Angew. Chem. Int. Ed. Engl. 33 (1994) 384.
[4] A.-L. Barra, D. Gatteschi, L. Pardi, A. Muller, I. Dorning, J. Am. Chem. Soc. 114 (1992) 8509.
[5] J.B. Vincent, G. Christou, Adv. Inorg. Chem. 33 (1989) 197.
[6] W. Heisenberg, Z. Phys. 49 (1928) 619.
[7] K. Kambe, J. Phys. Soc. Jpn. 5 (1950) 481.
[8] H. Kobayashi, T. Haseda, E. Kanda, S. Kanda, J. Phys. Soc. Jpn. 18 (1963) 349.
[9] J.B. Goodenough, Phys. Chem. Solids 6 (1955) 287.
[10] J. Kanamori, Phys. Chem. Solids 10 (1959) 87.
[11] K. Yamaguchi, Chem. Phys. Lett. 30 (1975) 288.
[12] K. Yamaguchi, Y. Yoshioka, T. Fueno, Chem. Phys. 20 (1977) 171.
[13] T. Lis, Acta Crystallogr. Sect. B 36 (1980) 2042.
[14] A. Caneschi, D. Gatteschi, R. Sessoli, A.L. Barra, L.C. Brunel, M. Guillot, J. Am. Chem. Soc. 113 (1991) 5873.
[15] R. Sessoh, H.-L. Tsai, A.R. Schake, S. Wang, J.B. Vincent, K. Folting, D. Gatteschi, G. Cbristou, D.N. Hendrickson, J. Am. Chem. Soc. 115 (1804) 1993.
[16] R. Sessoli, D. Gatteschi, A. Caneschi, M.A. Novak, Nature 365 (1993) 141.
[17] C. Paulsen, J.-G. Paxk, B. Barbara, R. Sessoli, A. Caneschi, J. Magn. Magn. Mater. 140–144 (1891) 1995.
[18] L. Thomas, F. Lionti, R. Ballou, D. Gatteschi, R. Sessoli, B. Barbara, Nature 383 (1996) 145.
[19] J.L. Van Hemmen, A. Sütö, Physica 141B (1986) 37.
[20] E.M. Chudnovsky, L. Gunther, Phys. Rev. Lett. 60 (1988) 661.
[21] E. Fradkin, M. Stone, Phys. Rev. B38 (1988) 7215.
[22] E. Manousakis, Rev. Mod. Phys. 63 (1991) 1.
[23] M. Nishino, H. Nagao, Y. Yoshioka, K. Yamaguchi, Mol. Cryst. Liq. Cryst., 335 (1999) 593.
[24] J. von Delft, C.L. Henley, Phys. Rev. Lett. 69 (1992) 3236.
[25] D. Loss, D.P. DiVincenzo, G. Grinstein, Phys. Rev. Lett. 69 (1992) 3232.
[26] H. Nagao, S. Yamanaka, M. Nishino, Y. Yoshioka, K. Yamaguchi, Chem. Phys. Lett. 302 (1999) 418.
[27] R. Rajaraman, Solitons and Instantons, North-Holland, Amsterdam, 1987.
[28] J. Klauder, Phys. Rev. D 19 (1979) 2349.
[29] F.D.M. Haldane, Phys. Rev. Lett. 57 (1986) 1488.

[30] F.D.M. Haldane, Phys. Rev. Lett. 61 (1988) 1029.
[31] F. Keffer, T. Oguchi, Phys. Rev. 115 (1959) 1428.
[32] N.L. Huang, R. Orbach, Phys. Rev. 154 (1967) 487.
[33] P.J. Hay, J.C. Thibeault, R. Hoffman, J. Am. Chem. Soc. 97 (1975) 4884.
[34] O. Kahn, B. Briat, J. Chem. Soc. Faraday Trans. 72 (1976) 268.
[35] K. Yamaguchi, S. Yabushita, T. Fueno, S. Kato, K. Morokuma:and, S. Iwate, Chem. Phys. Lett. 71 (1980) 563.
[36] P. de Loth, P. Cassoux, J.P. Daudey, J.P. Matrieu, J. Am. Chem. Soc. 103 (1981) 4007.
[37] K. Iberle, E.R. Davidson, J. Chem. Phys. 76 (1982) 5385.
[38] H. Astheimer, W. Haase, J. Chem. Phys. 85 (1986) 1427.
[39] J. Miralles, O. Castell, R. Caballol, J.P. Malrieu, Chem. Phys. 172 (1993) 33.
[40] O. Castell, J. Miralles, R. Caballol, Chem. Phys. 179 (1994) 377.
[41] C. Wang, K. Fink, V. Staemmler, Chem. Phys. 192 (1995) 25.
[42] P.W. Anderson, Phys. Rev. 115 (1959) 2.
[43] P.W. Anderson, Solid State Phys. 14 (1963) 99.
[44] L. Hedin, B. Lundqvist, J. Phys. C 4 (1971) 2064.
[45] U. von Barth, L. Hedin, J. Phys. C 5 (1972) 1629.
[46] K. Yamaguchi, T. Fueno, H. Fukutome, Chem. Phys. Lett. 22 (1973) 460.
[47] (a) K. Yamaguchi, Chem. Phys. Lett. 33 (1975) 330. (b) K. Yamaguchi, Chem. Phys. Lett. 66 (1979) 395.
[48] L. Noodleman, J.G. Norman Jr., J. Chem. Phys. 70 (1979) 4903.
[49] A.P. Ginsberg, J. Am. Chem. Soc. 102 (1980) 111.
[50] L. Noodleman, J. Chem. Phys. 74 (1981) 5737.
[51] A. Aizman, D.A. Case, J. Am. Chem. Soc. 104 (1982) 3269.
[52] K. Yamaguchi, Y. Takahaxa, T. Fueno, in: V.H. Smith, et al. (Eds.), Applied Quantum Chemistry, Reidel, Dordrecht, 1986, p. 155.
[53] L. Noodleman, E.R. Davidson, Chem. Phys. 109 (1985) 131.
[54] A. Bencini, D. Gatteschi, J. Am. Chem. Soc. 108 (1980) 5763.
[55] K. Yamaguchi, Y. Takahara, T. Fueno, K. Nasu, Jpn. J. Appl. Phys. 26 (1987) L1362.
[56] K. Yamaguchi, T. Tsunekawa, Y. Toyoda, T. Fueno, Chem. Phys. Lett. 143 (1988) 371.
[57] K. Yamaguchi, T. Fueno, N. Ueyama, A. Nakamura, M. Ozaki, Chem. Phys. Lett. 164 (1989) 1210.
[58] J.G. Norman Jr., P.B. Ryan, L. Noodleman, J. Am. Chem. Soc. 102 (1980) 4279.
[59] L. Noodleman, A.D. Case, Adv. Inorg. Chem. 38 (1992) 423.
[60] S. Yamanaka, T. Kawakami, H. Nagao, K. Yamaguchi, Chem. Phys. Lett. 231 (1994) 25.
[61] J.R. Hait, A.K. Rappe, S.M. Gorun, T.H. Upton, J. Phys. Chem. 96 (1992) 6264.
[62] K. Yamaguchi, M. Okumura, K. Takada, S. Yamanaka, Int. J. Quant. Chem. 27 (1993) 501, and references therein.
[63] M. Nishino, S. Yamanaka, Y. Yoshioka, K. Yamaguchi, J. Phys. Chem. A101 (1997) 705.
[64] E. Ruiz, P. Alemany, S. Alvarez, J. Cano, J. Am. Chem. Soc. 119 (1997) 1297.
[65] A. Bencini, F. Totti, C.A. Daul, K. Doclo, P. Fantucci, V. Barone, Inorg. Chem. 36 (1997) 5022.
[66] E. Ruiz, J. Cano, S. Alvarez, P. Alemany, J. Comp. Chem. 20 (1999) 1391.
[67] A. Matteo, V. Baxone, J. Phys. Chem. A103 (1999) 7676.
[68] E. Libby, R.J. Webb, W.E. Streib, K. Folting, J.C. Huffman, D.N. Hendrickson, G. Christou, Inorg. Chem. 28 (1989) 4037.
[69] J.M. Hernandez, X.X. Zhang, F. Luis, J. Tejada, J.R. Friedinan, M.P. Sarachik, R. Ziolo, Phys. Rev. B 55 (1997) 5858.
[70] D.A. Gaxanin, E.M. Chudnowky, Phys. Rev. B 56 (1997) 11102.
[71] H. De Raedt, S. Miyashita, K. Saito, D. Garcia-Pablos, N. Garcia, Phys. Rev. B 56 (1997) 11761.
[72] C.J. Bardley, A.P. Cracknell, The Mathematical Theory of Symmetry in Solids, Clarendon Press, Oxford, 1972.
[73] K. Yamaguchi, T. Fueno, M. Ozaki, N. Ueyama, A. Nakamura, Chem. Phys. Lett. 168 (1990) 56.
[74] K. Yamaguchi, S. Yamanaka, M. Nishino, Y. Takano, Y. Kitagawa, H. Nagao, Y. Yoshioka, Theoret. Chem. Acc. 102 (1999) 328.

[75] E. Fradkin, Field Theories of Condensed Matter Systems, Addison-Wesley, Reading, MA, 1991 (Chapter 5).
[76] M.W. Wemple, H.-L. Tsai, K. Folting, D.N. Hendrickson, G. Christou, Inorg. Chem. 32 (1993) 2025.
[77] H. Nagao, K. Nishikawa, S. Aono, Chem. Phys. Lett. 190 (1992) 97.
[78] H. Nagao, K. Nishikawa, S. Aono, Chem. Phys. Lett. 215 (1993) 5.
[79] H. Nagao, K. Nishikawa, K. Yamaguchi, S. Aono, 315 (1999) 441.
[80] Y. Fujii, T. Goto, K. Awaga, T. Okuno, Y. Sasaki, T. Mizusaki, J. Magn. Magn. Mater. 177–181 (1998) 991.
[81] D. Gatteschi, A. Caneschi, L. Pardi, R. Sessoli, Science 265 (1994) 1054.
[82] K.L. Taft, C.D. Delfs, G.C. Papaefthymiou, S. Foner, D. Gatteschi, S.J. Lippard, J. Am. Chem. Soc. 116 (1994) 823.
[83] M. Dupuis, A. Marquez, E.R. Davidson, HONDO-95.3 from CHEM-STATION, IBM, Kingston, NY, 1995.
[84] M.J. Frisch, G.W. Trucks, H.B. Schlegel, P.M.W. Gill, B.G. Johnson, M.A. Robb, J.R. Cheeseman, T.A. Keith, G.A. Peterssoid, J.A. Montgomery, K. Raghavachari, M.A. Al-Laham, V.G. Zakrzewski, J.V. Ortiz, J.B. Foresman, J. Cioslowski, B.B. Stefanov, A. Nanayakkara, M. Challacombe, C.Y. Peng, P.Y. Ayala, W. Chen, M.W. Wong, J.L. Andres, E.S. Replogle, R. Gomperts, R.L. Martin, D.J. Fox, J.S. Binkley, D.J. Defrees, J. Baker, J.P. Stewart, M. Head-Gordon, C. Gonzalez, J.A. Pople, GAUSSIAN-94, Gaussian, Pittsburgh, PA, 1995.
[85] H. Nagao, Y. Shigeta, H. Kawabe, T. Kawakami, K. Nishikawa, K. Yamaguchi, J. Chem. Phys. 107 (1997) 6283.
[86] H. Nagao, H. Kawabe, T. Kawakami, M. Okumura, W. Mori, K. Nishikawa, K. Yamaguchi, Mol. Cryst. Liq. Cryst. 286 (1996) 171.
[87] T. Kawakami, H. Nagao, K. Ueda, W. Mori, K. Yamaguchi, Mol. Cryst. Liq. Cryst. 286 (1996) 177.
[88] T. Kawakami, H. Nagao, W. Mori, K. Yamaguchi, Synth. Met. 85 (1997) 1753.
[89] Y. Shigeta, T. Kawakami, H. Nagao, K. Yamaguchi, Chem. Phys. Lett. 315 (1999) 441.
[90] H. Kawabe, H. Nagao, K. Nishikawa, Int. J. Quant. Chem. 60 (1997) 538.
[91] A. Caneschi, D. Gatteschi, C. Sangregorio, R. Sessoli, L. Sorace, Private communication at ICMM, Seihnosse le Penon, France, 1998.
[92] W. Wernsdorfer, R. Sessoli, Science 284 (1999) 133.
[93] R.P. Feynnian, Int. J. of Theoret. Phys. 21 (1982) 467.
[94] P. Beninoff, J. Stat. Phys. 29 (1982) 515.
[95] D. Deutsch, Proc. R. Soc. Lond. A400 (1985) 96.
[96] D. Deutsch, Proc. R. Soc. Lond. A425 (1989) 73.
[97] R. Landauer, Found. Phys. 16 (1986) 551.
[98] C. Bennett, IBM J. Res. Dev. 17 (1973) 525.
[99] N.A. Gershenfeld, I.L. Chaung, Science 275 (1997) 350.
[100] M. Nakano, K. Yamaguchi, Trends Chem. Phys. 5 (1997) 87.
[101] J. Limburg, J.S. Vrettos, L.M. Liable-Sands, A.L. Rheigold, T.H. Crabtree, G.W. Brudvig, Science 283 (1999) 1524.
[102] P.E.M. Siegbahn, R.H. Crabtree, J. Am. Chem. Soc. 121 (1999) 117.
[103] H. Basch, K. Mogi, D.G. Musaev, K. Morokuma, J. Am. Chem. Soc. 121 (1999) 7249.
[104] Y. Yoshioka, S. Kubo, K. Yamaguchi, I. Saito, Chem. Phys. Lett. 294 (1998) 459.